

# Room-Temperature Ferroelectricity in Hexagonally Layered $\alpha$ - $\text{In}_2\text{Se}_3$ Nanoflakes down to the Monolayer Limit

Fei Xue,\* Weijin Hu, Ko-Chun Lee, Li-Syuan Lu, Junwei Zhang, Hao-Ling Tang, Ali Han, Wei-Ting Hsu, Shaobo Tu, Wen-Hao Chang, Chen-Hsin Lien, Jr-Hau He, Zhidong Zhang, Lain-Jong Li,\* and Xixiang Zhang\*

2D ferroelectric material has emerged as an attractive building block for high-density data storage nanodevices. Although monolayer van der Waals ferroelectrics have been theoretically predicted, a key experimental breakthrough for such calculations is still not realized. Here, hexagonally stacking  $\alpha$ - $\text{In}_2\text{Se}_3$  nanoflake, a rarely studied van der Waals polymorph, is reported to exhibit out-of-plane (OOP) and in-plane (IP) ferroelectricity at room temperature. Ferroelectric multidomain states in a hexagonal  $\alpha$ - $\text{In}_2\text{Se}_3$  nanoflake with uniform thickness can survive to 6 nm. Most strikingly, the electric-field-induced polarization switching and hysteresis loop are, respectively, observed down to the bilayer and monolayer ( $\approx 1.2$  nm) thicknesses, which designates it as the thinnest layered ferroelectric and verifies the corresponding theoretical calculation. In addition, two types of ferroelectric nanodevices employing the OOP and IP polarizations in 2H  $\alpha$ - $\text{In}_2\text{Se}_3$  are developed, which are applicable for nonvolatile memories and heterostructure-based nanoelectronics/optoelectronics.

## 1. Introduction

Ferroelectricity, a property of materials intrinsically preserving the spontaneous polarization that can be switched by an applied electric field, has extensive applications, including nonvolatile memories<sup>[1–4]</sup> and high-performance transistors.<sup>[5,6]</sup> Currently, the most technologically and scientifically important ferroelectrics are  $\text{ABO}_3$ -structured perovskite ceramics,<sup>[7,8]</sup> such

as  $\text{BaTiO}_3$ ,  $\text{PbTiO}_3$ , and  $\text{BiFeO}_3$ . Because of their 3D crystallization, ultrathin and high-quality ferroelectric films for nanodevice applications can be produced solely through epitaxial growth on certain lattice-matched substrates.<sup>[1–4]</sup> However, such strict material preparation is commonly accompanied by extra strain due to lattice mismatch and rich surface defects or dangling bonds in the obtained ultrathin samples,<sup>[9]</sup> which impedes the development of interface-assembling ferroelectric heterostructures or electronics toward miniaturization.

The 2D van der Waals ferroelectric crystals offer the complementary features of ultrathin geometry, free of dangling bonds across the interface, and easy manipulation for integration with other materials.<sup>[10]</sup>

Together with other functionalities, including unique semiconducting, optical, and piezoelectric characters, layered 2D ferroelectrics have ignited growing interest in both theoretical and experimental research community.<sup>[10–14]</sup> Currently, Liu et al. reduced the ferroelectric thickness in layered  $\text{CuInP}_2\text{S}_6$  crystal to 4 nm and demonstrated its Curie transition temperature of 320 K.<sup>[15]</sup> Zhou et al. reported that the rhombohedral  $\alpha$ - $\text{In}_2\text{Se}_3$  crystal is an out-of-plane (OOP) polarized ferroelectric at room temperature.<sup>[16]</sup> Furthermore,


Dr. F. Xue, Dr. J. Zhang, H.-L. Tang, Dr. A. Han, S. Tu, Prof. L.-J. Li, Prof. X. Zhang  
Physical Sciences and Engineering Division  
King Abdullah University of Science and Technology  
Thuwal 23955-6900, Saudi Arabia  
E-mail: xuefei0828@gmail.com; ljliv@tsmc.com;  
xixiang.zhang@kaust.edu.sa

Dr. W. Hu, Prof. Z. Zhang  
Shenyang National Laboratory for Materials Science  
Institute of Metal Research (IMR)  
Chinese Academy of Sciences (CAS)  
Shenyang 110016, China  
K.-C. Lee, Prof. C.-H. Lien  
Institute of Electronics Engineering  
National TsingHua University  
Hsinchu 30013, Taiwan

L.-S. Lu, Dr. W.-T. Hsu, Prof. W.-H. Chang  
Department of Electrophysics  
National Chiao Tung University  
Hsinchu 30010, Taiwan

Prof. J.-H. He  
Computer, Electrical, and Mathematical  
Sciences and Engineering Division  
King Abdullah University of Science and Technology  
Thuwal 23955-6900, Saudi Arabia

Prof. L.-J. Li  
Corporate Research and Chief Technology Office  
Taiwan Semiconductor Manufacturing Company (TSMC)  
Hsinchu 30075, Taiwan

 The ORCID identification number(s) for the author(s) of this article can be found under <https://doi.org/10.1002/adfm.201803738>.

DOI: 10.1002/adfm.201803738

our group has confirmed the intercorrelated OOP and in-plane (IP) ferroelectric polarization switching in a (CVD)-synthesized rhombohedral  $\alpha$ - $\text{In}_2\text{Se}_3$  crystal with a thickness of 6 nm.<sup>[17]</sup> However, the thickness of polarization switching for layered ferroelectrics has not yet experimentally reached the challenging but intriguing monolayer limit.

Semiconducting  $\alpha$ - $\text{In}_2\text{Se}_3$  has two stacking forms: a rhombohedral (3R) structure and a hexagonal (2H) structure. Popovic et al. pointed out their discrepancy in lattice parameters using X-ray Diffraction (XRD) measurement in 1971.<sup>[18,19]</sup> Our previous work has confirmed this polymorphism and proposed an atom model for 2H $\alpha$ - $\text{In}_2\text{Se}_3$  via scanning transmission electron microscope (STEM), electron diffraction, and XRD analysis.<sup>[20]</sup> The prediction of OOP and IP ferroelectricity in  $\alpha$ - $\text{In}_2\text{Se}_3$ <sup>[11]</sup> and the experimental advances in 3R-structured counterparts<sup>[17]</sup> motivated us to explore whether the hexagonally stacking  $\alpha$ - $\text{In}_2\text{Se}_3$  is ferroelectric. Surprisingly, we find that the exfoliated 2H $\alpha$ - $\text{In}_2\text{Se}_3$  nanoflakes virtually maintain stable ferroelectricity in the OOP and IP orientations at room temperature. Ferroelectric multidomain states are observed at a homogeneous thickness as thin as 6 nm. Moreover, we obtain ferroelectric polarization switching and hysteresis loop, respectively, down

to the bilayer and monolayer levels from this 2H  $\alpha$ - $\text{In}_2\text{Se}_3$ , which demonstrates that it is the thinnest layered ferroelectric. Two types of  $\alpha$ - $\text{In}_2\text{Se}_3$  nanodevices based on the OOP and IP polarizations are also developed. As a layered ferroelectric semiconductor, 2H  $\alpha$ - $\text{In}_2\text{Se}_3$  presents a possibility for the development of high-density nonvolatile memories and multifunctional heterostructures.

## 2. Results and Discussion

The 2H  $\alpha$ - $\text{In}_2\text{Se}_3$  nanoflakes were directly cleaved from the bulk crystal onto a conductive substrate (Au 20 nm/Si wafer) for the following piezoelectric force microscopy (PFM) characterizations. As **Figure 1a** illustrates, atom-force-microscope (AFM) images depict the exfoliated typical monolayer, trilayer, and quadrilayer  $\alpha$ - $\text{In}_2\text{Se}_3$  nanoflakes. Each monolayer with five atom planes (Se-In-Se-In-Se, quintuple layer) has a thickness of  $\approx 1.2$  nm (see the height profiles in Figure S1 of the Supporting Information), which is consistent with previous works.<sup>[16,21]</sup> Evidently, the substrate surface of the e-beam-deposited gold layer is relatively rough with a height variation of  $\approx 2.5$  pm,

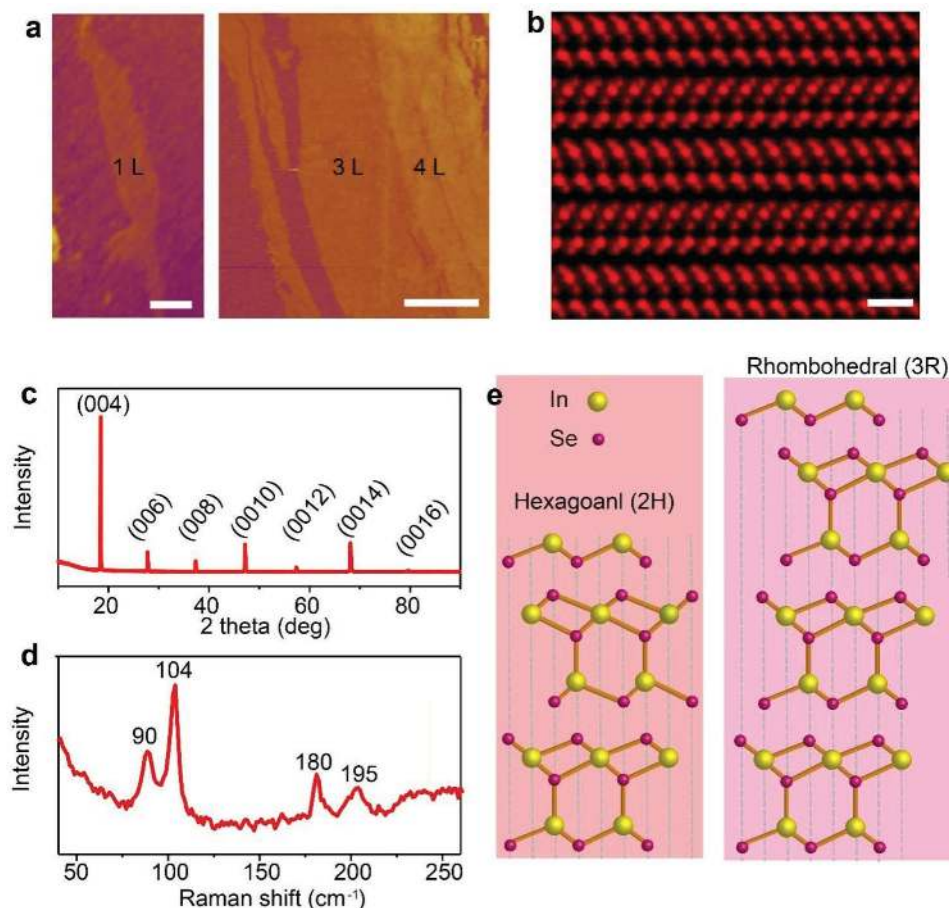


**Figure 1.** Characterizations of 2H  $\alpha$ - $\text{In}_2\text{Se}_3$  nanoflakes. a) AFM images of the exfoliated ultrathin  $\alpha$ - $\text{In}_2\text{Se}_3$  nanoflakes. Scale bar: 300 nm for the left-side image and 1  $\mu\text{m}$  for the right-side image. b) Cross-sectional high-resolution STEM image of a  $\alpha$ - $\text{In}_2\text{Se}_3$  nanoflake. Scale bar: 1 nm. c) XRD pattern for the used bulk  $\alpha$ - $\text{In}_2\text{Se}_3$  crystal. d) Raman spectra of a multilayer  $\alpha$ - $\text{In}_2\text{Se}_3$  nanoflake. e) Side-view model of  $\alpha$ - $\text{In}_2\text{Se}_3$  atom structure; for comparison, the right panel displays the 3R structure.

which causes the topography of atom-thick  $\alpha$ -In<sub>2</sub>Se<sub>3</sub> to be uneven. High-resolution STEM was used to characterize the 2H crystal structure as indicated in Figure 1b. From this cross-sectional view and the atom structure model in the left panel of Figure 1e, it is clear that the unit cell for the 2H  $\alpha$ -In<sub>2</sub>Se<sub>3</sub> crystal contains two quintuple layers, with the upper (or the bottom) layer flipping over. This stacking feature is unambiguously distinct from the 3R counterpart (a unit cell that consists of three shifted quintuple layers), as displayed in Figure 1e, which suggests that our samples should belong to another polymorphic form of  $\alpha$ -In<sub>2</sub>Se<sub>3</sub>, namely a 2H structure.

To confirm this claim, XRD patterns and Raman spectra were successively employed to examine the  $\alpha$ -In<sub>2</sub>Se<sub>3</sub> crystal. Notably, the large-sized samples with a *c*-plane normal to the substrate were used in the XRD measurement. The diffraction pattern, as shown in Figure 1c, exhibits the *c*-plane peak and high-order interplanar spacing, thereby enabling us to determine the lattice constant *c* ( $\approx 19.235$  Å). Such parameter is highly consistent with that reported for 2H $\alpha$ -In<sub>2</sub>Se<sub>3</sub>, which is obviously distinguishable from that of 3R $\alpha$ -In<sub>2</sub>Se<sub>3</sub> ( $28.76 \pm 0.007$  Å).<sup>[18,22–24]</sup> Figure 1d depicts the typical Raman spectra for the used  $\alpha$ -In<sub>2</sub>Se<sub>3</sub> crystal, which reveal four remarkable peaks at 90, 104, 180, and 195 cm<sup>-1</sup>. These peaks are respectively attributed to the E, A(LO+TO), A(TO), and A(TO) phonon modes.<sup>[25]</sup> It is worth noting that in comparison with the Raman spectra of the 3R structure,<sup>[16,17,26,27]</sup> the 2H $\alpha$ -In<sub>2</sub>Se<sub>3</sub> crystal always presents an extra splitting peak at 90 cm<sup>-1</sup>, which can be considered as an indication of 2H stacking. In general, our intensive characterizations strongly support that the  $\alpha$ -In<sub>2</sub>Se<sub>3</sub> crystal in this work should be assigned to the 2H structure.

The non-centrosymmetric nature of the 2H  $\alpha$ -In<sub>2</sub>Se<sub>3</sub> crystal has been confirmed by the second harmonic generation (SHG) and PFM measurements,<sup>[20]</sup> which provides a necessary requirement for the emergence of ferroelectricity in the 2H  $\alpha$ -In<sub>2</sub>Se<sub>3</sub> crystal. From the perspective of the atomic model, the 2H structure maintains an upper-five-atom-plane layer rotated 180° from the bottom one along the *c* axis as shown in Figure 1e, whose configuration does not break the special atom arrangement that ferroelectricity requires in the 3R polymorph. On the other hand, Ding et al. have predicted that monolayer In<sub>2</sub>Se<sub>3</sub> exhibits room-temperature ferroelectricity in both OOP and IP orientations. Thus, we can expect that 2H  $\alpha$ -In<sub>2</sub>Se<sub>3</sub> crystal should be ferroelectric as well.

To investigate the ferroelectric polarization of the exfoliated 2H  $\alpha$ -In<sub>2</sub>Se<sub>3</sub> nanoflakes, PFM was used. The PFM amplitude and PFM phase are closely associated with the local electromechanical response and polarization direction of a ferroelectric domain, respectively. To facilitate comprehension of the results, the AFM topographic image and related height profile of a typical 2H  $\alpha$ -In<sub>2</sub>Se<sub>3</sub> nanoflake with a thickness ranging from 12 nm to sub-6 nm are shown in Figure 2a,b. We have noticed that the substrate is slightly tilted, which commonly and inevitably occurs during the tip-scanning processes but does not affect the following ferroelectric investigation. Figure 2c,d displays the OOP PFM amplitude and phase measured by the vertical motions of the AFM probe for the previously presented ultrathin sample. Overall, there are two large distinct regions with a 180° phase change that correspond to the up and down spontaneously polarized domains in the OOP direction. These results

preliminarily indicate that the 2H  $\alpha$ -In<sub>2</sub>Se<sub>3</sub> crystal is ferroelectric. As the images clearly illustrate, the bean-like domain walls are formed along not only the border of areas with different thicknesses but also the homogeneous surface. When conducting the PFM measurements, we noted that domain reversal easily occurred in regions with different thicknesses (Figure S2, Supporting Information); however, as the labeled triangular area reveals (Figure 2a), it still can be maintained in an ultrathin sample with homogeneous thickness of 6 nm. It was additionally noted that the inclined dark strip in the bean-shaped domain area (Figure 2d) should be ascribed to the height discrepancy.

The IP ferroelectric polarization for the typical 2H  $\alpha$ -In<sub>2</sub>Se<sub>3</sub> nanoflake was also measured by the twisting motions of AFM probe as shown in Figure 2d,e. The virtual existence of IP spontaneous polarization can be understood from the inequivalent interlayer spacings between the central Se atom layer and the adjacent two In atom layers (left panel of Figure 1e). The shape, size, and location of the corresponding domain wall agree well with that in the OPP images (Figure 2a,b), thereby demonstrating the coupling effect between the OOP and IP polarizations. It is noteworthy that the jump of the AFM probe caused the bottom area of the bean-shaped domain and its neighbor in Figure 2f to closely entangle.

Ferroelectric materials should respond to an applied electric field and further display a polarization change. We next applied a poling voltage to the AFM probe to investigate local ferroelectric switchable behaviors. Figure 3a,b shows the OOP and IP PFM phase changes for a typical 30 nm sample after writing with +7 V DC bias in the large square and -8 V DC bias in the inner small pattern. The images that were collected from a bilayer (2.3 nm) sample under the same experimental conditions are shown in Figure 3d,e. The relevant height profiles and PFM amplitude are orderly presented in Figures S3 and S4 (Supporting Information). The clear evidence of the bias modulated polarization effect further validates the existence of intrinsic ferroelectricity in the 2H $\alpha$ -In<sub>2</sub>Se<sub>3</sub> ultrathin layer. More importantly, the pronounced phase reversal confirms that the switching of polarization in van der Waals ferroelectric  $\alpha$ -In<sub>2</sub>Se<sub>3</sub> can be achieved down to the bilayer (2.3 nm). It is notable that the OOP phase transition is always accompanied by the IP phase change, which can be explained by the lateral movement of central Se atom layers (Figure S5, Supporting Information) as the theoretical work has predicted.<sup>[11]</sup> Such intercorrelated behavior in 2H  $\alpha$ -In<sub>2</sub>Se<sub>3</sub> is akin to that in 3R  $\alpha$ -In<sub>2</sub>Se<sub>3</sub> due to its analog structure.<sup>[17]</sup> Moreover, we conducted the corresponding ferroelectric retention test as shown in Figure S6 (Supporting Information). The written domain pattern remains stable and minimally fading, even after 72 h at ambient conditions, which firmly excludes some possible contributions from charge accumulation or electrochemical phenomenon. In addition, Raman spectra (Figure S7, Supporting Information) is used to confirm that 2H  $\alpha$ -In<sub>2</sub>Se<sub>3</sub> does not undergo a chemical modification before and after DC bias poling.

Figure 3c,f show the related off-field piezoresponse hysteresis loops for the 30-nm sample (Figure 3a) and 2.3-nm bilayer sample (Figure 3d). The parallelogram-like piezoresponse loops, as signature characteristics of ferroelectrics, quantitatively reflect the detailed process of local ferroelectric domain reversal for 2H $\alpha$ -In<sub>2</sub>Se<sub>3</sub>. The positive writing DC bias (7 V) compels the

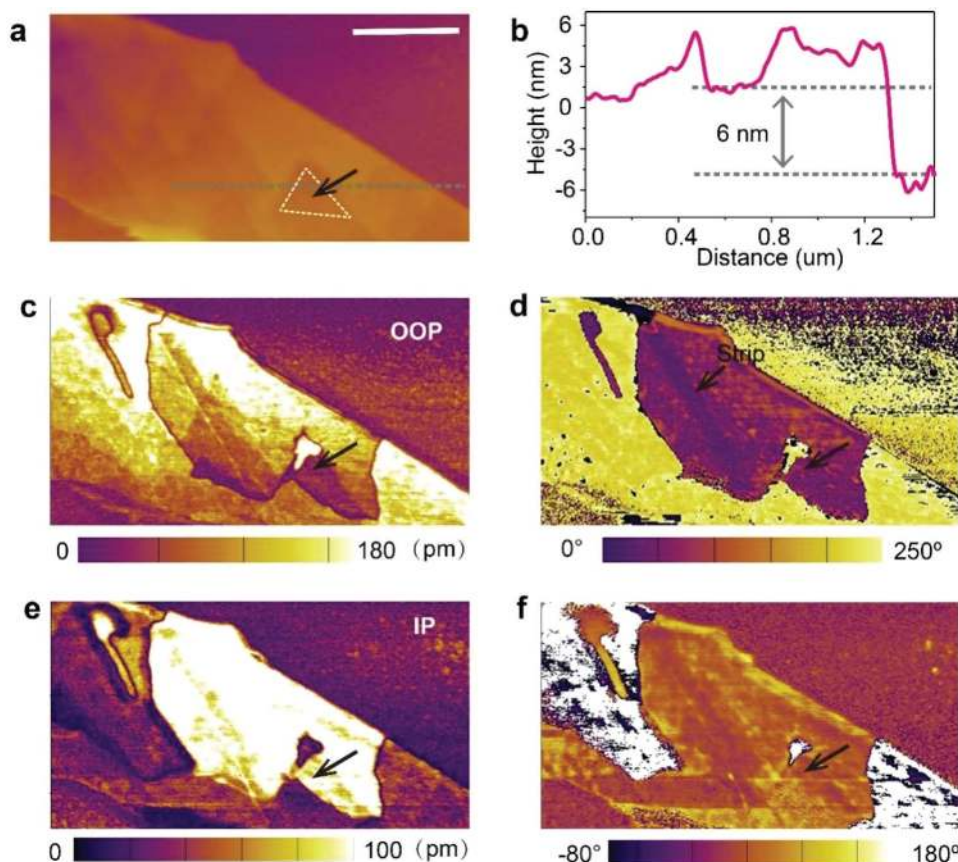


**Figure 2.** PFM study of a typical 2H  $\alpha$ -In<sub>2</sub>Se<sub>3</sub> nanoflake. a) AFM image for an  $\alpha$ -In<sub>2</sub>Se<sub>3</sub> specimen with a thickness ranging from  $\approx 12$  to  $\approx 5$  nm. Scale bar: 500 nm. b) The height profile for the dashed gray line in (a), which indicates that the triangular-like area labeled by the black arrow has a thickness of  $\approx 6$  nm. c) The corresponding OOP PFM amplitude and d) PFM phase. e) The related IP PFM amplitude and f) PFM phase. The highlighted areas in (a) and (c–f) indicate that the ferroelectric multidomain states can survive in a homogeneous thickness of 6 nm.

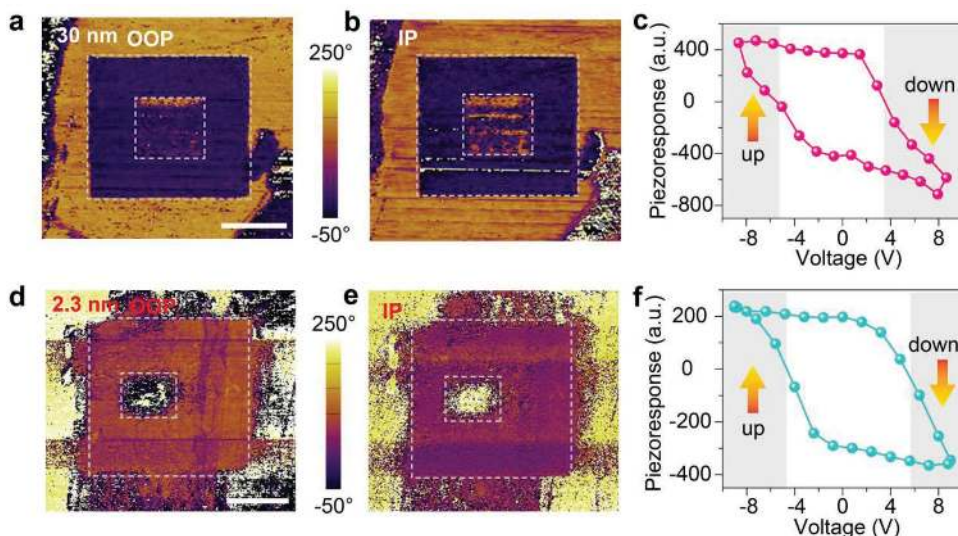


**Figure 3.** Ferroelectric switching for the 2H  $\alpha$ -In<sub>2</sub>Se<sub>3</sub> nanoflakes. a) The OOP and b) IP PFM phases with the forward and reverse DC bias written in the box patterns and c) the local ferroelectric hysteresis loop for a 30-nm  $\alpha$ -In<sub>2</sub>Se<sub>3</sub> flake. d) The OOP and e) IP PFM phases after 7 V and  $-8$  V bias writing and f) the local switching loop for a 2.3-nm (bilayer)  $\alpha$ -In<sub>2</sub>Se<sub>3</sub> flake. Scale bar: 1  $\mu$ m; writing voltage: +7 V for large square and  $-8$  V for small inner square; the arrows in (c) and (f) represent the ferroelectric polarization directions.

domain polarization downward; similarly, the negative writing voltage ( $-8$  V) forces the domain polarization upward, as the arrows indicate. As previously reported,<sup>[16,28]</sup> the slight shift or offset of the hysteresis loops is presumably caused by the asymmetrical Schottky barriers between the top and bottom electrodes or the polar defects imprinted to the original polarization. To demonstrate the reliability of our PFM system, ultrathin non-ferroelectric centrosymmetric  $\beta$ - $\text{In}_2\text{Se}_3$  were measured under the same experimental conditions. The results (Figure S8, Supporting Information) do not show any obvious piezoresponses that are akin in 2H  $\alpha$ - $\text{In}_2\text{Se}_3$ , which validate that our obtained ferroelectric behaviors are not caused by the electrostatic effect between AFM tip and samples. In a word, combining with the spontaneous domain walls, responses to external bias, switching loops, and long retention time, we can conclude that 2H  $\alpha$ - $\text{In}_2\text{Se}_3$  nanoflake is an intrinsic ferroelectric stemming from its internal non-centrosymmetry. Note that the thickness dependence of non-centrosymmetry induced piezoelectric behaviors for 2H  $\alpha$ - $\text{In}_2\text{Se}_3$  has been systematically investigated in the previous work.<sup>[20]</sup>

SHG measurement is a reliable tool to probe noncentrosymmetric properties for studying intrinsic ferroelectrics.<sup>[15]</sup> The corresponding SHG dependence on azimuthal angles for a multilayer 2H  $\alpha$ - $\text{In}_2\text{Se}_3$  is shown in Figure 4a, which exhibits a nonzero  $C_3$  symmetry. Such noncentrosymmetric feature is due to the coherent interference of OOP  $C_\infty$  symmetry and IP  $C_6$  symmetry,<sup>[20]</sup> revealing that the intrinsically broken symmetry results in the ferroelectric polarizations in OOP and IP orientations. Figure 4b shows SHG intensity of a multilayer  $\alpha$ - $\text{In}_2\text{Se}_3$  before and after anneal. If not specified, all anneal conditions are at 573 K for 30 min. Significantly, the specimen after anneal does not exhibit any SHG intensity because of its transformation to a centrosymmetric phase, namely  $\beta$ - $\text{In}_2\text{Se}_3$ . This distinct discrepancy in SHG intensity before and after anneal verifies that  $\alpha$ - $\text{In}_2\text{Se}_3$  evolves from a ferroelectric phase to a paraelectric phase with increasing temperature, a typical signature of ferroelectrics. The temperature dependence of SHG intensity is shown in Figure S9 of the Supporting Information, which demonstrates that the ferroelectric-spontaneous polarization for  $\alpha$ - $\text{In}_2\text{Se}_3$  can remain robust up to 360 K.

As for the monolayer 2H  $\alpha$ - $\text{In}_2\text{Se}_3$ , the representative ferroelectric switching loops (piezoresponse hysteresis loops) that were measured at two spots on the sample are exhibited in Figure 5. Note that such loops have been examined on seven monolayered specimens, thus validating theoretical predictions that room-temperature ferroelectricity can overcome the surface-charge-induced depolarization field and be maintained in the monolayer limit.<sup>[11]</sup> This should be the first experimental observation of ferroelectricity in a monolayer van der Waals material. With its combination of unique semiconducting and optical properties, monolayer  $\alpha$ - $\text{In}_2\text{Se}_3$  ferroelectric provides a new research platform or direction for exploring functional device application and underlying physical principles. Because of the weak van der Waals force between the small-sized

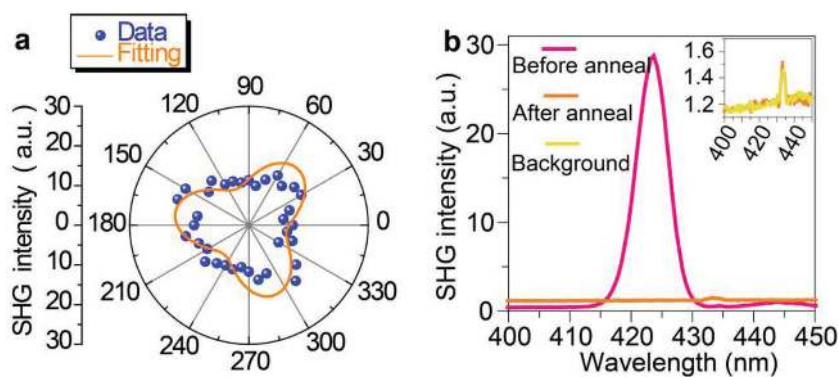


**Figure 4.** SHG characterization. a) SHG intensity as a function of sample azimuthal angle for a 2H  $\alpha$ - $\text{In}_2\text{Se}_3$  nanoflake. The fitting curve in yellow is also shown. b) SHG intensity from a multilayer  $\alpha$ - $\text{In}_2\text{Se}_3$  before and after anneal. The background is also plotted for comparison.

monolayer (the left panel of Figure 5) and the gold substrate, PFM tip can easily damage or even peel off the samples when scanning back and forth, so it is difficult or impossible to record the switching phase image, as shown in Figure 3a.

To demonstrate its application to nonvolatile memories, we fabricated 1) a switchable ferroelectric diode that consists of vertically stacked n-type  $\alpha$ - $\text{In}_2\text{Se}_3$  and p-type Si; 2) a planar  $\alpha$ - $\text{In}_2\text{Se}_3$  nanodevice. Silver paste and the AFM conductive tip, respectively, act as the bottom and top electrodes for vertically prototypical device (see the inset of Figure 6a). Using a conductive AFM measurement, the typical IV curves (Figure 6a) were designedly obtained from a 10-nm ferroelectric  $\alpha$ - $\text{In}_2\text{Se}_3$ -based heterostructure device. It is apparent that when applying a negative bias to the n-type  $\alpha$ - $\text{In}_2\text{Se}_3$  (the p-type Si is grounded), this diode displays forward conduction and excellent rectifying property. Importantly, we can observe a remarkable hysteresis and current (resistance) switching, which should result from the OOP polarization switching of the 2H  $\alpha$ - $\text{In}_2\text{Se}_3$ , as evidenced in Figures 2 and 3. The two highly overlapped electrical curves with voltage bias sweeping back and forth twice confirm that the switching effect is stable and reproducible. When the applied negative voltage for the p–n diode exceeds the related negative coercive voltage of approximately  $-4.5$  V, the current (resistance) switching takes place. Additionally,

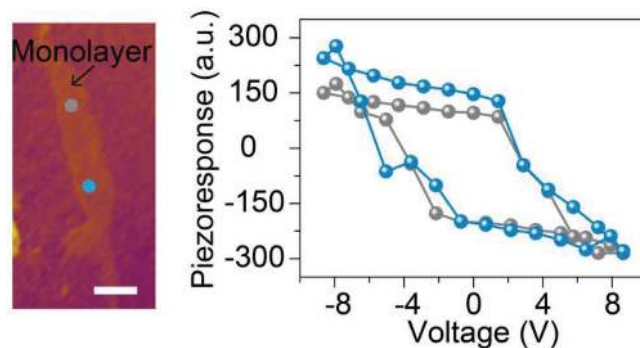


**Figure 5.** Ferroelectric hysteresis loops in the monolayer limit ( $\approx 1.2$  nm) of 2H  $\alpha$ - $\text{In}_2\text{Se}_3$  crystal. The typical monolayer  $\alpha$ - $\text{In}_2\text{Se}_3$  flake is shown in the left panel and two switching loops, displayed in the right panel are, respectively, acquired from the corresponding spots as the color guides. Scale bar: 300 nm.

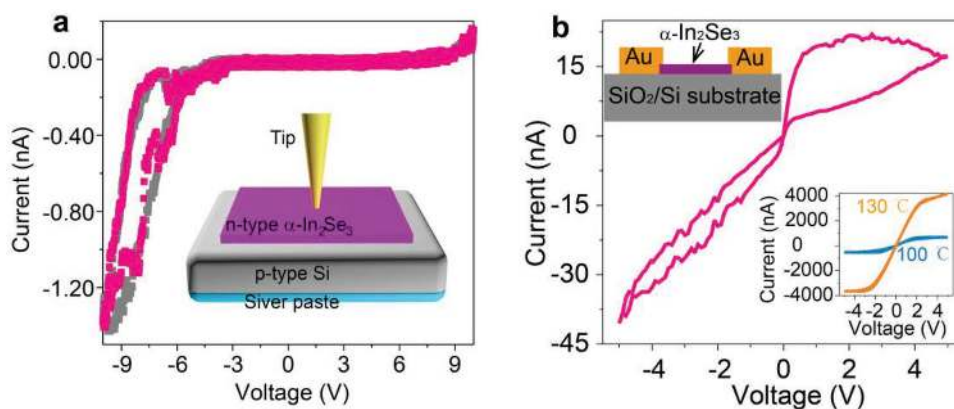


**Figure 6.** Demonstration of  $\alpha$ - $\text{In}_2\text{Se}_3$ -based ferroelectric devices. a) Electrical curves for a vertically stacked p–n heterojunction with voltage bias sweeping back and forth twice. The inset shows a detailed configuration of the switchable diode, in which 2H  $\alpha$ - $\text{In}_2\text{Se}_3$  thickness is about  $\approx 10$  nm. b) Electrical curves for a planar  $\alpha$ - $\text{In}_2\text{Se}_3$  nanodevice under room temperature (pink lines), 100 and 130 °C. The left inset shows the practical device configuration and the right inset exhibits IV curves at high temperature.

a planar  $\alpha$ - $\text{In}_2\text{Se}_3$  device also shows such switching effect (Figure 6b), which should originate from the IP ferroelectricity. As expected, the hysteresis in IV curves almost disappears at high temperature above 130 °C. With raising temperature, the carrier concentration of the semiconducting  $\alpha$ - $\text{In}_2\text{Se}_3$  drastically increases and the screening effect on polarization charges from carriers can largely boost. Thereby, the current hysteresis induced by ferroelectric polarization charges could collapse at high temperature.

### 3. Conclusion

In conclusion, we report that the hexagonal  $\alpha$ - $\text{In}_2\text{Se}_3$  crystal is ferroelectric both in the OOP and IP orientations at room temperature. Ferroelectric multidomain states in a homogeneous-thickness  $\alpha$ - $\text{In}_2\text{Se}_3$  flake can be realized in a thickness as low as 6 nm. The polarization switching and hysteresis loops are, respectively, observed down to the bilayer and monolayer thicknesses, which designates it as the thinnest layered ferroelectric. In addition, we demonstrate two kinds of prototype ferroelectric nanodevices that are based on vertical and lateral polarizations in  $\alpha$ - $\text{In}_2\text{Se}_3$ , which can be used in nonvolatile and advanced electronics.

### 4. Experimental Section

Raman measurement was performed using a 532-nm excitation laser (WITec alpha 300 confocal Raman microscopy). PFM measurement was conducted on Cypher ES-Asylum Research Oxford Instruments under a contact and dual-AC resonance mode. The bulk 2H  $\text{In}_2\text{Se}_3$  crystal was bought from 2D Semiconductors. The conductive substrates (30 nm Au/500  $\mu\text{m}$  Si) that directly support the 2H  $\text{In}_2\text{Se}_3$  nanoflakes were grounded to perform all the PFM characterizations. A soft conductive tip with a Pt/Ti coating and a spring average constant of 3 N/m was employed. The contact resonance frequencies for OOP and IP measurement were  $\approx 320$  and  $\approx 1200$  kHz, respectively. An AC voltage of 0.5–1 V was applied to measure the hysteresis loop. SHG measurement was carried out using a Ti:sapphire femtosecond-pulsed laser (1050 nm) by a homemade optical microscope in the backscattering condition.

### Supporting Information

Supporting Information is available from the Wiley Online Library or from the author.

### Acknowledgements

F.X., W.H., and K.-C.L. contributed equally to this work. The research presented here was supported by King Abdullah University of Science and Technology (KAUST) Office of Sponsored Research (OSR) under Award No: CRF-2015-2634-CRG4, and CRF-2016-2996-CRG5. W.J.H thanks the support from the “Hundred Talents Program” of the Chinese Academy of Sciences. W.-H.C. acknowledges the support from the Ministry of Science and Technology (MOST) of Taiwan (105-2119-M-009-014-MY3, 107-2112-M-009-024-MY3) and the Center for Emergent Functional Matter Science (CEFMS) of NCTU.

### Conflict of Interest

The authors declare no conflict of interest.

### Keywords

hexagonal  $\alpha$ - $\text{In}_2\text{Se}_3$ , layered 2D materials, monolayer, room-temperature ferroelectricity

Received: May 30, 2018  
Revised: September 27, 2018  
Published online:

- [1] A. Chanthbouala, A. Crassous, V. Garcia, K. Bouzouane, S. Fusil, X. Moya, J. Allibe, B. Dlubak, J. Grollier, S. Xavier, C. Deranlot, A. Moshar, R. Proksch, N. D. Mathur, M. Bibes, A. Barthelemy, *Nat. Nanotechnol.* **2012**, *7*, 101.
- [2] A. Chanthbouala, V. Garcia, R. O. Cherif, K. Bouzouane, S. Fusil, X. Moya, S. Xavier, H. Yamada, C. Deranlot, N. D. Mathur, M. Bibes, A. Barthelemy, J. Grollier, *Nat. Mater.* **2012**, *11*, 860.
- [3] V. Garcia, S. Fusil, K. Bouzouane, S. Enouz-Vedrenne, N. D. Mathur, A. Barthelemy, M. Bibes, *Nature* **2009**, *460*, 81.

- [4] H. Lu, C. W. Bark, D. E. de los Ojos, J. Alcalá, C. B. Eom, G. Catalan, A. Gruverman, *Science* **2012**, 336, 59.
- [5] L. Liao, H. J. Fan, B. Yan, Z. Zhang, L. L. Chen, B. S. Li, G. Z. Xing, Z. X. Shen, T. Wu, X. W. Sun, J. Wang, T. Yu, *ACS Nano* **2009**, 3, 700.
- [6] M. W. Si, C. J. Su, C. S. Jjiang, N. J. Conrad, H. Zhou, K. D. Maize, G. Qiu, C. T. Wu, A. Shakouri, M. A. Alam, P. D. Ye, *Nat. Nanotechnol.* **2018**, 13, 24.
- [7] W. J. Hu, Z. H. Wang, W. L. Yu, T. Wu, *Nat. Commun.* **2016**, 7, 10808.
- [8] Y. W. Yin, J. D. Burton, Y. M. Kim, A. Y. Borisevich, S. J. Pennycook, S. M. Yang, T. W. Noh, A. Gruverman, X. G. Li, E. Y. Tsybal, Q. Li, *Nat. Mater.* **2013**, 12, 397.
- [9] M. H. Yusuf, B. Nielsen, M. Dawber, X. Du, *Nano Lett.* **2014**, 14, 5437.
- [10] A. Belianinov, Q. He, A. Dziazgys, P. Maksymovych, E. Eliseev, A. Borisevich, A. Morozovska, J. Banys, Y. Vysochanskii, S. V. Kalinin, *Nano Lett.* **2015**, 15, 3808.
- [11] W. J. Ding, J. B. Zhu, Z. Wang, Y. F. Gao, D. Xiao, Y. Gu, Z. Y. Zhang, W. G. Zhu, *Nat. Commun.* **2017**, 8, 14956.
- [12] R. Fei, W. Kang, L. Yang, *Phys. Rev. Lett.* **2016**, 117, 097601.
- [13] M. H. Wu, X. C. Zeng, *Nano Lett.* **2017**, 17, 6309.
- [14] Y. Wang, C. Xiao, M. Chen, C. Hua, J. Zou, C. Wu, J. Jiang, S. A. Yang, Y. Lu, W. Ji, *Mater. Horiz.* **2018**, 5, 521.
- [15] F. C. Liu, L. You, K. L. Seyler, X. B. Li, P. Yu, J. H. Lin, X. W. Wang, J. D. Zhou, H. Wang, H. Y. He, S. T. Pantelides, W. Zhou, P. Sharma, X. D. Xu, P. M. Ajayan, J. L. Wang, Z. Liu, *Nat. Commun.* **2016**, 7, 12357.
- [16] Y. Zhou, D. Wu, Y. H. Zhu, Y. J. Cho, Q. He, X. Yang, K. Herrera, Z. D. Chu, Y. Han, M. C. Downer, H. L. Peng, K. J. Lai, *Nano Lett.* **2017**, 17, 5508.
- [17] C. Cui, W. J. Hu, X. Yan, C. Addiego, W. Gao, Y. Wang, Z. Wang, L. Li, Y. Cheng, P. Li, X. Zhang, H. N. Alshareef, T. Wu, W. Zhu, X. Pan, L. J. Li, *Nano Lett.* **2018**, 18, 1253.
- [18] S. Popovic, B. Celustka, D. Bidjin, *Phys. Status Solidi A* **1971**, 6, 301.
- [19] S. Popovic, A. Tonejc, B. Grzetaplenkovic, B. Celustka, R. Trojko, *J. Appl. Crystallogr.* **1979**, 12, 416.
- [20] F. Xue, J. Zhang, W. Hu, W.-T. Hsu, A. Han, S.-F. Leung, J.-K. Huang, Y. Wan, S. Liu, J. Zhang, J.-H. He, W.-H. Chang, Z. L. Wang, X. Zhang, L.-J. Li, *ACS Nano* **2018**, 12, 4976.
- [21] J. Zhou, Q. Zeng, D. Lv, L. Sun, L. Niu, W. Fu, F. Liu, Z. Shen, C. Jin, Z. Liu, *Nano Lett.* **2015**, 15, 6400.
- [22] C. H. Ho, C. H. Lin, Y. P. Wang, Y. C. Chen, S. H. Chen, Y. S. Huang, *ACS Appl. Mater. Interfaces* **2013**, 5, 2269.
- [23] K. Kambas, C. Julien, M. Jouanne, A. Likforman, M. Guittard, *Phys. Status Solidi B* **1984**, 124, K105.
- [24] R. B. Jacobs-Gedrim, M. Shanmugam, N. Jain, C. A. Durcan, M. T. Murphy, T. M. Murray, R. J. Matyi, R. L. Moore, B. Yu, *ACS Nano* **2014**, 8, 514.
- [25] R. Lewandowska, R. Bacewicz, J. Filipowicz, W. Paszkowicz, *Mater. Res. Bull.* **2001**, 36, 2577.
- [26] X. Tao, Y. Gu, *Nano Lett.* **2013**, 13, 3501.
- [27] D. Wu, A. J. Pak, Y. N. Liu, Y. Zhou, X. Y. Wu, Y. H. Zhu, M. Lin, Y. Han, Y. Ren, H. L. Peng, Y. H. Tsai, G. S. Hwang, K. J. Lai, *Nano Lett.* **2015**, 15, 8136.
- [28] C. T. Nelson, P. Gao, J. R. Jokisaari, C. Heikes, C. Adamo, A. Melville, S. H. Baek, C. M. Folkman, B. Winchester, Y. J. Gu, Y. M. Liu, K. Zhang, E. G. Wang, J. Y. Li, L. Q. Chen, C. B. Eom, D. G. Schlom, X. Q. Pan, *Science* **2011**, 334, 968.